

Why is second-order vision less efficient than first-order vision?

Velitchko Manahilov ^{a,*}, William A. Simpson ^b, Julie Calvert ^a

^a *Department of Vision Sciences, Glasgow Caledonian University, Cowcaddens Road, Glasgow G4 0BA, UK*

^b *Simulation and Modelling Section, DRDC Toronto, 1133 Sheppard Avenue West, Toronto, Ont., Canada M3M 3B9*

Received 23 February 2004; received in revised form 29 November 2004

Abstract

Research has shown that the sensitivity to second-order modulations of carrier contrast is lower than that to first-order luminance modulations stimuli. We sought to compare the efficiency of processing first- and second-order information. Employing a phase-discrimination paradigm we found that when humans were given sufficient a priori information of signal parameters they detected both luminance and contrast modulations of 0.6 and 2 c/deg by a phase-sensitive algorithm. The overall detection efficiency for second-order patterns, however, was lower than that for first-order stimuli. To study the factors which limit the efficiency of first- and second-order vision, we measured detection performance for luminance and contrast modulations of 0.6 and 2 c/deg embedded in Gaussian noise. The results showed that the detection of second-order patterns had lower sampling efficiency and higher additive internal noise as compared to the detection of first-order stimuli. Classification images for detecting contrast modulations of 2 c/deg resembled the side-band component of the contrast modulations which suggests that human observers may detect contrast modulations of a sinusoidal carrier using first-order luminance channels. The lower sensitivity of the mechanism detecting second-order patterns might be due to higher levels of additive internal noise and lower sampling efficiency than those of the mechanism analysing first-order patterns.

© 2005 Elsevier Ltd. All rights reserved.

Keywords: Second-order vision; Efficiency; Noise

1. Introduction

In everyday experience, the visual system is exposed to a stream of information that is likely to be incomplete and noisy. Our ability to extract information from these incomplete and noisy sensory messages is limited by various factors: the level of internal noise due to randomness of neural activity, the sampling efficiency with which humans use the available stimulus information, signal parameter uncertainty effects, and non-linear operations in the visual system (for review see Burgess, 1990). Efficiency can be characterised by measuring human performance and comparing it to the best possible performance of an ideal observer (Tanner & Birdsall,

1958). This approach has been used successfully to understand the sources of inefficiency of human performance in the detection of visual objects defined by a pattern of luminance in space and time (Barlow, 1978; Eckstein, Ahumada, & Watson, 1997; Legge, Kersten, & Burgess, 1987; Lu & Doshier, 1999; Pelli, 1990; Simpson, Falkenberg, & Manahilov, 2003).

We know little, however, about performance efficiency in the detection of visual objects which are defined by second-order modulations of carrier contrast. Contrast modulations can be produced if a sine grating, referred to as the carrier, is multiplied by another sine grating of the same orientation but much lower spatial frequency. This results in a grating of the carrier spatial frequency whose contrast is modulated sinusoidally at the modulating spatial frequency. Second-order information usually occurs in combination with first-order luminance information. In some natural situations, however,

* Corresponding author. Tel.: +44 141 331 8204; fax: +44 141 331 3387.

E-mail address: vma@gcal.ac.uk (V. Manahilov).

such as shadows handling transparency, second-order information is particularly useful (Daugman & Downing, 1995).

The main difference between processing of these two types of information is that the modulation sensitivity to second-order patterns is lower than the contrast sensitivity to first-order stimuli (Manahilov, Calvert, & Simpson, 2003; Schofield & Georgeson, 1999, 2000). The modulation depths of both patterns, however, are not identical quantities as they are defined by different algorithms. For example, the signal amplitude of contrast modulations depends on the carrier contrast level. Here we compared the efficiencies of first- and second-order vision and studied the factors that underlie performance for detecting luminance and contrast modulations.

The ideal observer uses all the available a priori information of the image and makes a decision based on the most probable hypothesis (Green & Swets, 1974). When a signal is embedded in Gaussian white noise with zero mean and the ideal observer knows the form of the expected signal exactly, the most efficient strategy is cross-correlation of the received stimulus with a template which is a copy of the signal. Burgess and Ghandeharian (1984) showed that when humans were given sufficient a priori information of signal parameters, their performance for detecting luminance signals exceeded that of the less efficient energy detector and was consistent with a cross-correlation strategy. We do not know whether human performance for detection of contrast modulations is also based on such a cross-correlation algorithm or whether it uses a less-efficient energy algorithm. We employed a phase-discrimination paradigm (Burgess & Ghandeharian, 1984) to test these two possibilities.

Sampling efficiency and internal noise of a real observer can be estimated using the equivalent input noise approach which is based on measuring how the signal contrast energy required for an observer to maintain a given performance level depends on the amount of external visual noise added to the signal (Nagaraja, 1964; Pelli, 1990). We estimated the internal noise and sampling efficiency of the first- and second-order pathways by using the equivalent input noise approach in conjunction with models developed by Lu and Doshier (1999) and Eckstein et al. (1997). To determine the relevant stimulus features used by human observers in the detection of contrast modulations, we estimated the response classification images to second-order patterns using the response classification technique (for a review see Ahumada, 2002).

2. Methods

2.1. Apparatus and stimuli

The stimuli were generated by a Pentium 3 computer on a 19" RGB monitor at a screen resolution of

640 × 480 pixels and a frame rate of 120 Hz. The stimuli were displayed using a 256-colour look-up table and a 12-bit grey-scale resolution obtained by a video summation device according to Pelli and Zhang (1991). The mean luminance was 30 cd/m². The monitor's gamma non-linearity was linearized carefully and the calibration was verified every few weeks. The stimuli were displayed in two fields (1.5 × 1.5 deg), presented above and below a central dark fixation point and separated vertically by 1 deg. The contrast of the patterns in the lower and upper edges of each field was damped by a cosine function (half-period of 1 deg) in order to reduce the effects of spatial transients at the stimulus edges. The viewing distance was 2 m.

We used luminance and contrast modulations of 0.6 and 2 c/deg. Fig. 1 illustrates stimuli of 2 c/deg: (1) a pedestal—a 3-cycle vertical sinusoidal grating (Fig. 1a), (2) a signal—a 1-cycle vertical sinusoidal grating having different phase shifts (θ) relative to the pedestal (Fig. 1b: $\theta = 0$ deg; c: $\theta = 112.5$ deg and d: $\theta = 180$ deg) and (3) a high-frequency component—a vertical sinusoidal grating of 10 c/deg and 0.3 contrast (Fig. 1e). First-order modulations were generated by summation of the pedestal, the signal and the high-frequency component (Fig. 1f–h). The high-frequency component and the pedestal were presented in the whole stimulation field, while the 1-cycle signal was shown in the central part of the stimulation field (Fig. 1—grey bar). The luminance profile of the first-order stimulus in the central 0.5 deg part of the stimulation field was

$$I(x, y) = I_0[1 + C \sin(2\pi x f_c) + M \sin(2\pi x f_m + \theta) + P \sin(2\pi x f_m)], \quad (1)$$

where I_0 is mean luminance, C and f_c are the contrast and spatial frequency of the high-frequency grating, M

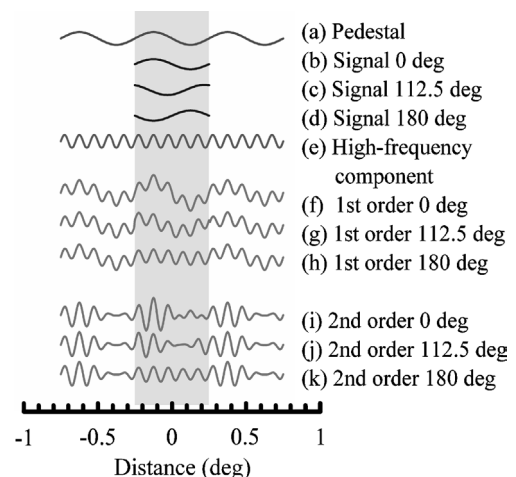


Fig. 1. One-dimensional plot of the stimuli of 2 c/deg: (a) A pedestal sinusoidal grating of 2 c/deg; (b–d) 2 c/deg modulation signal of three spatial phases; (e) a sinusoidal grating of 10 c/deg; (f–h) first-order modulations; (i–k) second-order modulations.

and P are the contrasts of the signal and pedestal and f_m is the spatial frequency of both signal and pedestal.

Contrast modulations consisted of a carrier (the high-frequency component) whose contrast was modulated by the sum of the pedestal and the signal (Fig. 1i–k). The luminance profile of the second-order stimulus in the central 0.5 deg part of the stimulation field was

$$I(x, y) = I_0 \{ 1 + C \sin(2\pi x f_c) + C \sin(2\pi x f_c) \times [M \sin(2\pi x f_m + \theta) + P \sin(2\pi x f_m)] \}. \quad (2)$$

The term $C \sin(2\pi x f_c)$ represents the carrier and the term $C \sin(2\pi x f_c) [M \sin(2\pi x f_m + \theta) + P \sin(2\pi x f_m)]$ denotes the side-band component which comprises two sinusoids with frequencies close to that of the carrier.

In the case of patterns of 0.6 c/deg, the width of both the pedestal and signal was 1 cycle. The stimuli were embedded in static 2D Gaussian white noise whose Gaussian distribution was clipped at 2.5 standard deviations. Two types of noise were used: different—in each trial, different noise samples were displayed in both stimulation fields and fixed—in all trials of an experimental session, a single noise sample was shown in the upper and lower fields. The noise pixel size was 2.6×2.6 min arc.

2.2. Procedures

In preliminary experiments, detection thresholds were measured using a staircase method and a spatial two-alternative forced-choice (2AFC) procedure (for details see Manahilov et al., 2003) designed to determine 79% correct responses (Levitt, 1971). The stimuli contained only a signal without a pedestal ($P = 0$). First- and second-order stimuli were used in different sessions. In each trial, different noise samples of $9.5 \mu\text{deg}^2$ density were shown in each stimulation field. 0.5 s after the trial onset, two stimuli of 1 s duration were added to the noise samples. One of the stimuli contained a signal; the other one had no signal. The observer's task was to identify the field that contained the signal by pressing one of two buttons.

In Experiments 1 and 2, we used the 2AFC procedure to measure the percentage of correct responses. This score (P_c) was transformed into the detectability index (d') by using the relation $d' = 2^{1/2} z(P_c)$, where z is the inverse of the normal distribution function (Macmillan & Creelman, 1991, pp. 121–126). For each condition, at least 300 trials were collected in three experimental sessions.

2.3. Response classification technique

We estimated classification images for detecting luminance signals and contrast modulations of a sinusoidal carrier. In 2 AFC experiments, both fields contained a 10-c/deg grating of 0.3 contrast. In the case of first-order patterns, the signal was a 1-cycle vertical grating of 2 c/deg which was added randomly to one of the stimulation fields. In the case of second-order patterns, the

contrast of one randomly selected field was modulated by a 1-cycle grating of 2 c/deg. In both conditions, Gaussian one-dimensional (vertical) white noise samples were added to the stimulation fields. The horizontal size of each noise element was equal to the screen pixel size (0.88 min of arc). The noise standard deviation was 0.15. The modulation-depth level of the first-order patterns was 0.063 and that of the second-order patterns were 0.79. Under these conditions, the observers' proportion of correct responses was within the range of 0.74–0.80.

One-dimensional classification images (K) were calculated using the method developed by Abbey and Eckstein (2002) for a 2AFC task:

$$K = \frac{1}{(n_t - 1)\sigma^2} \sum_{j=1}^{n_t} (o_j - \hat{P}_c)(n_j^+ - n_j^-), \quad (3)$$

where n_t is the number of trials, o_j is the observer score for the j th trial (if the observer correctly identified the signal-present image $o = 1$ and if the observer made an incorrect choice $o = 0$), n_j^+ and n_j^- are the signal-present and signal-absent images for the j th trial, respectively and $\hat{P}_c = \frac{1}{n} \sum_{j=1}^n o_j$ is the proportion of correct responses. Each classification image was based on 1200 trials obtained in two sessions. The classification images were spatially smoothed by a 5 point convolution kernel.

2.4. Statistical analysis

The goodness of the fit of model predictions to the data was estimated by an R^2 statistic which is the proportion of the variance accounted for by the fit, adjusted by the number of free parameters (Judd & McClelland, 1989). The R^2 value was calculated as follows:

$$R^2 = 1 - \left(\frac{\sum_{i=1}^n \frac{(\alpha_i - \alpha_{i\text{est}})^2}{n - k}}{\sum_{i=1}^n \frac{(\alpha_i - \alpha_{\text{ave}})^2}{n - 1}} \right), \quad (4)$$

where α_i represents the observed data values, $\alpha_{i\text{est}}$ denotes the model calculations, k is the number of free parameters, n is the number of data points and α_{ave} is the mean value of the experimental data.

2.5. Observers

Three observers took part in the experiment: two of the authors (JC and VM) and another observer (MF) who was not aware of the purpose of the experiments. All observers had normal or corrected-to-normal visual acuity and viewed the screen binocularly with natural pupils.

3. Results

3.1. Experiment 1

Burgess and Ghandeharian (1984) showed that when humans were given sufficient a priori information of

signal parameters, their performance for detecting luminance signals is based on a cross-correlation strategy and exceeds that of the less efficient energy detector. In this experiment we sought to understand whether human performance for detection of second-order patterns is based on such a cross-correlation algorithm or on a less-efficient energy algorithm.

In 2AFC experiments, the observer was presented with two fields consisting of a sinusoidal pedestal and a high-frequency component embedded in different 2D Gaussian noise samples of $9.5 \mu\text{deg}^2$ density. An incremental signal was displayed randomly in one of the stimulation fields. The spatial frequency of both the signal and pedestal was 0.6 or 2 c/deg. The observer had to select the stimulation field which contained the signal. In one set of experiments, the signal and the pedestal were contrast modulations of a sinusoidal carrier. In another set of the experiments they were luminance sinusoidal gratings. The luminance signals were added to a high-frequency grating of 10 c/deg to make the experimental conditions similar to those used in the experiment with contrast modulations which contained a high-frequency carrier.

In preliminary sessions, we measured the threshold contrast for detection of first- and second-order signals without a pedestal. For luminance and contrast modulations of 0.6 c/deg, the mean threshold contrasts and 95% confidence intervals were respectively: 0.018 ± 0.003 and 0.17 ± 0.02 (VM) and 0.017 ± 0.004 and 0.19 ± 0.03 (JC); for signals of 2 c/deg: 0.013 ± 0.0025 and 0.13 ± 0.025 (VM) and 0.0132 ± 0.0018 and 0.126 ± 0.02 (JC). In the main experiments, the contrast of the incremental signals was about 0.05 log units above the threshold contrasts for detection of the corresponding signals. The contrasts for luminance and contrast-modulated increments of 0.6 c/deg were 0.02 and 0.20; for increments of 2 c/deg they were 0.015 and 0.15, respectively. The contrast levels of the pedestal were 9/7 times higher than the contrast levels of the corresponding increments.

We measured percentage of correct responses for discriminating an incremental signal added to the pedestal as a function of the difference between the spatial phases of the signal and the pedestal. Fig. 2 shows the d' values for discriminating first- and second-order increments of 0.6 c/deg. Fig. 3 denotes the d' values for increments of 2 c/deg. The filled symbols illustrate the results for signal-pedestal phase differences of 0, 112.5, and 180 deg obtained in sessions in which the difference between the signal and pedestal phases varied randomly among nine values (0, 22.5, 45, 77.5, 90, 112.5, 135, 157.5, and 180 deg). For each observer, the d' values for both first- and second-order signals at a phase difference of 112.5 deg were not significantly different from zero. These findings are consistent with the predictions of an energy detector (see Appendix A). According to the

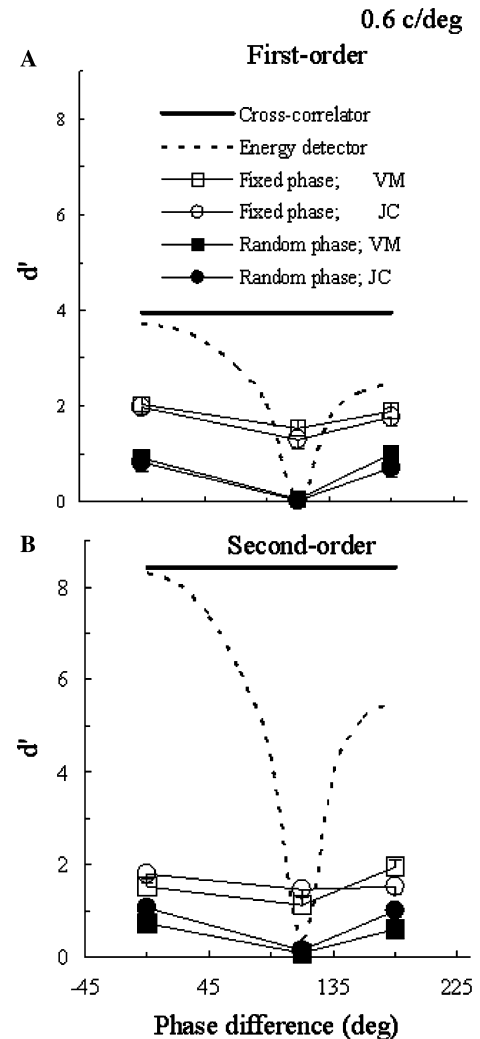


Fig. 2. Detectability index for discriminating luminance increments of 0.6 c/deg (A) and contrast-modulated increments 0.6 c/deg (B) embedded in different noise samples and superimposed on a pedestal as a function of signal-pedestal phase difference. Empty symbols—data obtained in signal-known-exactly conditions; filled symbols—data measured in random-phase conditions. Data from two observers. Thick lines— d' values of a cross-correlator; dotted lines— d' values of an energy detector. The vertical bars show 95% confidence interval.

energy model, when the increment and pedestal are in phase, the presence of the pedestal makes the performance of the energy detector essentially the same as the cross-correlator (Green & Swets, 1974, pp. 203–204). When the increment/pedestal contrast ratio is 7/9 and the phase difference is 112.5 deg, the performance of the energy detector drops to zero [Eq. (A.8)]. The dotted lines in Figs. 2 and 3 illustrate how the performance of the energy detector would depend on the phase difference. These results imply that when the observers are not given information of the signal phase they use a phase-insensitive algorithm to detect both first- and second-order patterns.

In a block of trials of another set of experiments, the signal-pedestal phase difference was fixed (0, 112.5, and

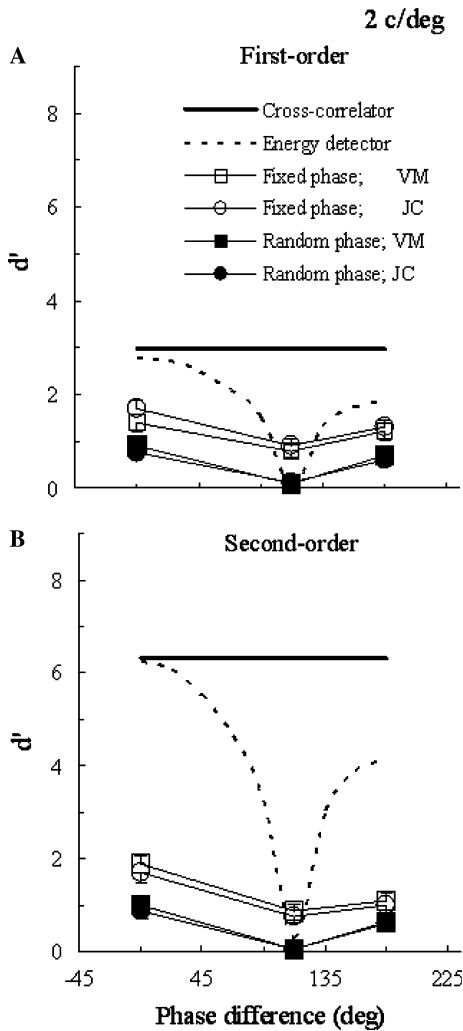


Fig. 3. Detectability index for discriminating luminance and contrast-modulated increments of 2 c/deg. The other designations are as in Fig. 2.

180 deg). The observers were given practice trials without external noise and they were able to choose the stimulation field containing the signal. Given a priori information of the signal phase, the d' values for both first- and second-order stimuli at 112.5 deg phase difference (Figs. 2 and 3, empty symbols) were significantly different from zero ($p < 0.001$). The observer performance does not approach the ideal-observer performance which shows that when observers are given sufficient a priori information, they can perform imperfect phase-sensitive detection.

For luminance signals, the performance of a cross-correlation detector [Eq. (A.2)] does not depend on the presence of the pedestal. The thick lines in Figs. 2A and 3A denote the detectability indexes predicted by the cross-correlation model for discriminating luminance increments. In Appendix A, we have described two models for discriminating contrast-modulated increments. The first one consists of a matching device

whose template is a copy of the difference between the contrast stimuli presented in both stimulation fields, which is the side-band component of the contrast modulations (Fig. 7A, Eq. (A.5)). Using Eq. (A.2) and the energy of this signal, we computed the model predictions presented by thick lines in Figs. 2B and 3B. The second model is based on the idea that second-order patterns are detected by a distinct second-order pathway (Cavanagh & Mather, 1989; Chubb & Sperling, 1988; Wilson, Ferrera, & Yo, 1992). The non-linear ideal-observer model consists of a non-linearity followed by a matching device which extracts the signal modulating the carrier contrast. The d' values predicted by this model were 10% lower than those calculated by the linear ideal-observer model. Therefore, we compared the performance of real observers to the predictions of the more efficient linear ideal-observer model.

The overall efficiency (η) for detection of first- and second-order patterns could be calculated by the relation (Tanner & Birdsall, 1958): $\eta = d_h^2/d_i^2$, where d_h is the detectability index measured under phase-sensitive detection and d_i is the detectability index of the ideal observer. The results averaged across observers and phase differences showed that contrast modulations of 0.6 c/deg were detected with 5.6 times (t -test, $p < 0.001$) lower overall efficiency ($\eta = 0.036 \pm 0.013$) than luminance gratings ($\eta = 0.2 \pm 0.06$). The overall efficiency for contrast modulations of 2 c/deg ($\eta = 0.042 \pm 0.03$) was 4.2 times (t -test, $p < 0.001$) lower than that for luminance gratings ($\eta = 0.18 \pm 0.09$).

The comparison between the performances in phase-certain and phase-uncertain conditions (phase 0 and 180 deg) showed that the d' values for these two conditions were significantly different ($p < 0.001$) for luminance and contrast modulations of 0.6 c/deg. The detectability indexes for luminance patterns of 2 c/deg were also significantly different ($p = 0.003$) while those for contrast modulations of 2 c/deg differed with a marginal probability of 0.054.

3.2. Experiment 2

The second experiment was designed to reveal the sources of inefficiency in detection of first- and second-order patterns.

Using the 2AFC procedure, we measured the performance for detection of first- and second-order signals of 0.6 and 2 c/deg embedded in Gaussian white noise whose density levels were 9.5, 18.9, and 28.4 μdeg^2 . The spatial phase of the sinusoidal signals was always zero in relation to the fixation point. The luminance and contrast-modulated signals had two modulation depth levels: C_a —those measured in the preliminary experiments and $C_b = C_a/2^{1/2}$. Detection performance was measured in the presence of two types of Gaussian white noise: (i) different—both stimulation fields in each

trial contained different noise samples and (ii) fixed—the upper and lower fields in all trials of an experimental session contained a single noise sample.

The estimated d' values for signals of 0.6 and 2 c/deg are shown in Figs. 4 and 5, respectively. The performance of our observers degraded as the noise density increased. The results show that the d' values for each signal modulation level in the presence of fixed noise were higher than those in different noise. The averaged ratio between the d' values measured with fixed and different noise samples was significantly larger (t -test, $p < 0.001$) for first-order signals of 0.6 c/deg (1.73 ± 0.12) and 2 c/deg (1.99 ± 0.13) as compared to those values for second-order modulations of 0.6 c/deg (1.46 ± 0.10) and 2 c/deg (1.42 ± 0.1). These findings indicate that the total internal noise, including the additive and multiplicative components, is higher for second-order signals than that for first-order modulations (Burgess & Colborne, 1988).

We fitted the data with two models for detection of visual stimuli (see Appendix B). The perceptual template model (PTM) (Lu & Dosher, 1999) and the elaborated linear amplifier model (ELAM) (Eckstein et al., 1997) assume that human performance is limited by suboptimal sampling efficiency, additive and multiplicative internal noises. The PTM approximates the nonlinear transducer function by a single nonlinearity, while the

ELAM assumes a linear transducer function and a decision process with stimulus uncertainties. The PTM has computational advantages in calculating sampling efficiency and internal noise, while the ELAM allows separating the effects of sampling efficiency and internal noise from those due to stimulus uncertainties.

The PTM [Eqs. (B.2) and (B.3)] have four free parameters (sampling efficiency k , the coefficient which determines the equivalent multiplicative noise m , the additive internal noise N_{add} and the exponent of the power transducer function γ). The ELAM has also four free parameters. The predictions of this model can be calculated by Eqs. (B.2) and (B.3), setting $\gamma = 1$. In addition to the parameters k , m , and N_{add} , the ELAM depends on the uncertainty number (U) corresponding to the irrelevant decision variables per location monitored by the observer. Using numerical evaluations of the integral in Eq. (B.4), we calculated d' for each performance level and for a range of U values (0–20). Table 1 represents the best-fitting free parameters of the PTM and those of the elaborated LAM calculated for different U values. For all experimental conditions, the R^2 values for the elaborated LAM were maximal at $U = 2$ and decreased at lower and higher U values. For all the experimental conditions, however, the R^2 values for the ELAM at $U = 2$ were slightly lower than the corresponding R^2 values obtained by the PTM.

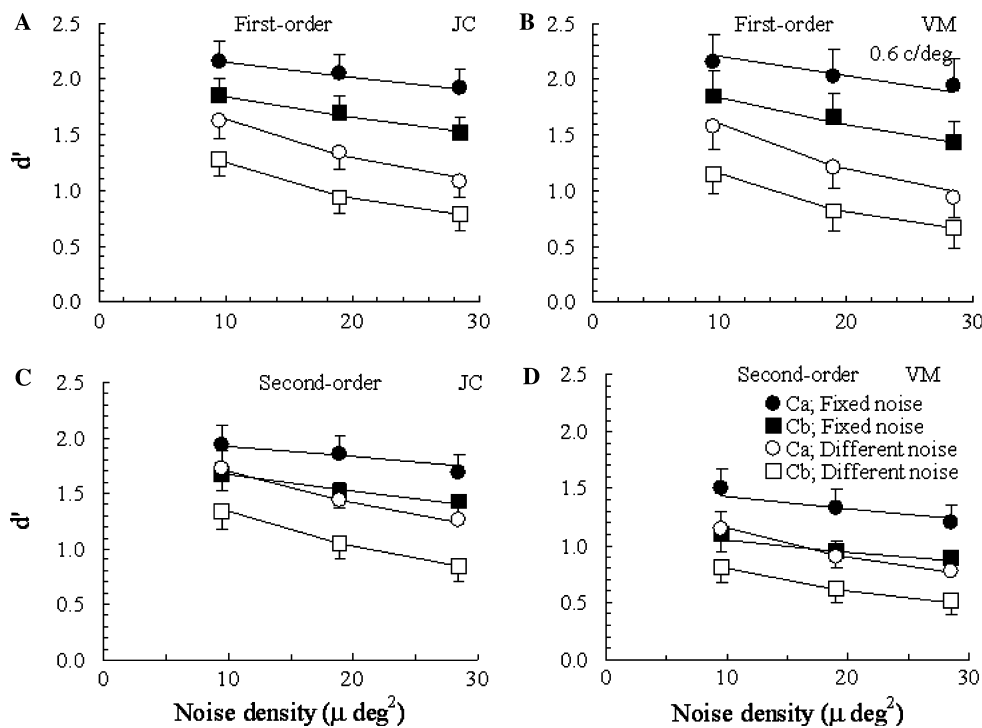


Fig. 4. Detectability index for detection of luminance signals (A and B) and contrast-modulated signals (C and D) of 0.6 c/deg embedded in different noise samples (empty symbols) and fixed noise samples (filled symbols) at various noise density. C_a and C_b —two modulation levels of the stimuli as described in the text. Lines denote the predictions of the PTM as explained in the text. Data from two observers. The vertical bars show 95% confidence interval.

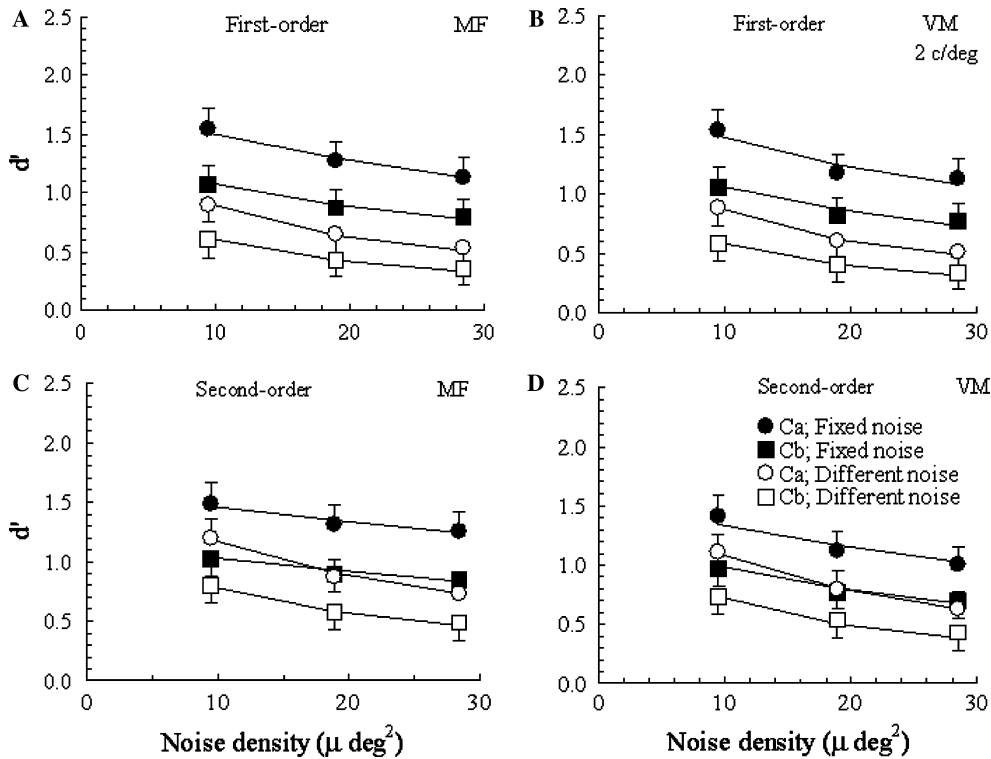


Fig. 5. Detectability index for detection of luminance signals and contrast-modulated signals of 2 c/deg. The other designations are as in Fig. 4.

Table 2 shows the averaged values across the observers and spatial frequencies of R^2 and the free parameters of both models used to fit the data. We compared the data for first- and second-order modulations using a paired t test. There were 10 paired comparisons and we used a Bonferroni correction to maintain the comparison-wise rate at $p = 0.05$. Thus, the minimum significance level was $p = 0.005$ ($0.05/10 = 0.005$). The PTM fitted the data with a slightly higher adjusted variance R^2 as compared with the fit of the elaborated LAM, however, the mean R^2 values were not significantly different. Both models showed that the sampling efficiency for the detection of second-order patterns was significantly lower by a factor of about four than that for the detection of first-order signals. In addition, the level of additive internal noise measured in detection of second-order modulations was significantly higher by a factor of about four than that estimated in detection of first-order patterns. It should be noted that the sampling efficiencies for both types of modulations calculated by the ELAM were about three times higher as compared to the sampling efficiencies for corresponding stimuli obtained by the PTM. The other parameters of the PTM (γ and m) and those of the elaborated LAM (U and m) for both first- and second-order signals were not significantly different.

3.3. Classification images

In the present study, we considered two ideal-observer models for detecting contrast modulations of a sinu-

soidal carrier in a 2AFC task (Appendix A). The template of the linear ideal-observer model is the side-band component of the second-order modulations (Fig. 7A); the template of the non-linear ideal-observer model has the waveform of the modulating signal (Fig. 7B, solid line). The analysis of our data was based on the comparison of the human performance with the ideal-observer performance. This analysis, however, does not determine how real observers perform the visual task. Such information could be obtained by means of the response classification technique developed by Ahumada and co-workers in audition (Ahumada & Lovell, 1971; Ahumada, Marken, & Sandusky, 1975) and vision (Ahumada, 1996). The response classification technique extracts linear image features which contribute to the detection of an image embedded in noise samples by correlating the noise samples with the observer's response. This experiment was aimed at establishing which parts of contrast-modulated patterns observers use to detect the stimulus.

Usually classification images are estimated using signals embedded in two-dimensional noise. The free parameters of such images are proportional to the number of pixels; thus a large number of trials is needed to get good estimates of the classification images. We estimated classification images for signals—vertical sinusoidal modulations, whose modulations were only in one dimension. To reduce the degrees of freedom in the data without losing important features, we used one-dimensional Gaussian vertical noise. The size of

Table 1

Best fitting values of the free parameters and the adjacent variance R^2 of the PTM and elaborated LAM used to fit the d' values for luminance and contrast modulations of 0.6 and 2 c/deg

		U	PTM	ELAM							
				0	1	2	3	4	5	10	20
<i>First-order 0.6 c/deg</i>											
JC	R^2		0.997	0.970	0.981	0.987	0.983	0.982	0.980	0.944	0.920
	γ		1.180	—	—	—	—	—	—	—	—
	m		0.154	0.133	0.123	0.107	0.102	0.098	0.094	0.083	0.073
	K		0.206	0.216	0.438	0.585	0.682	0.775	0.855	1.187	1.519
	N_{add}		3.7	3.2	3.5	3.0	4.2	4.3	4.5	5.2	5.7
VM	R^2		0.991	0.970	0.974	0.980	0.974	0.972	0.968	0.948	0.940
	γ		1.297	—	—	—	—	—	—	—	—
	m		0.140	0.129	0.111	0.101	0.095	0.088	0.086	0.076	0.069
	k		0.241	0.258	0.515	0.689	0.821	0.940	1.032	1.442	1.833
	N_{add}		4.0	2.2	3.1	3.6	3.7	4.1	4.2	4.8	5.1
2 c/deg	R^2		0.997	0.964	0.968	0.977	0.964	0.954	0.949	0.926	0.915
MF	γ		1.268	—	—	—	—	—	—	—	—
	m		0.148	0.167	0.154	0.151	0.142	0.130	0.117	0.108	0.091
	k		0.314	0.240	0.717	0.800	1.248	1.495	1.651	2.446	3.432
	N_{add}		4.0	1.4	3.1	3.2	3.4	4.1	4.5	5.1	6.2
VM	R^2		0.983	0.954	0.960	0.970	0.944	0.951	0.933	0.938	0.912
	γ		1.280	—	—	—	—	—	—	—	—
	m		0.159	0.180	0.181	0.163	0.149	0.141	0.136	0.114	0.098
	k		0.316	0.239	0.683	0.780	1.244	1.516	1.756	2.467	3.524
	N_{add}		3.6	1.0	2.0	2.8	3.1	3.6	4.1	4.6	5.8
<i>Second-order 0.6 c/deg</i>											
JC	R^2		0.992	0.936	0.948	0.955	0.942	0.933	0.935	0.926	0.911
	γ		1.410	1	1	1	1	1	1	1	1
	m		0.218	0.185	0.136	0.126	0.117	0.104	0.108	0.091	0.082
	k		0.060	0.077	0.155	0.206	0.247	0.279	0.304	0.403	0.531
	N_{add}		12.6	6.1	9.0	8.9	9.2	10.9	8.8	10.2	10.2
VM	R^2		0.984	0.931	0.958	0.963	0.942	0.931	0.926	0.917	0.905
	γ		1.320	1	1	1	1	1	1	1	1
	m		0.200	0.217	0.166	0.150	0.133	0.125	0.127	0.105	0.094
	k		0.040	0.033	0.094	0.130	0.158	0.183	0.203	0.298	0.399
	N_{add}		18.0	4.2	8.7	9.6	10.2	10.9	10.0	12.2	12.5
2 c/deg	R^2		0.992	0.932	0.948	0.957	0.944	0.943	0.940	0.930	0.913
MF	γ		1.440	1	1	1	1	1	1	1	1
	m		0.190	0.133	0.125	0.115	0.102	0.100	0.097	0.090	0.085
	k		0.082	0.074	0.199	0.272	0.337	0.386	0.437	0.625	0.887
	N_{add}		23.5	8.0	11.5	12.1	13.5	13.2	14.2	14.5	15.6
VM	R^2		0.978	0.866	0.864	0.884	0.865	0.843	0.858	0.840	0.831
	γ		1.557	1	1	1	1	1	1	1	1
	m		0.316	0.313	0.220	0.184	0.154	0.154	0.132	0.117	0.102
	k		0.076	0.060	0.180	0.252	0.324	0.352	0.410	0.603	0.811
	N_{add}		17.5	2.5	7.6	8.6	11.0	9.7	11.9	13.0	13.5

The free parameters of the ELAM were evaluated for various values of the uncertainty number U .

each stimulation field was 1.5×1.5 deg and the 1-cycle sinusoidal signal of 2 c/deg was displayed in the centre of the stimulation field.

Fig. 6 shows classification images for detecting luminance and contrast modulations of 2 c/deg, estimated by the method developed by Abbey and Eckstein (2002) for a 2AFC task. In accordance with previous studies (Ahumada, 2002 and others) we found that the waveform of classification images to a luminance grating (Fig. 6, A—observer JC, B—observer VM, and C—average) resemble the waveform of the signal (Fig. 6D). The amplitude of the classification images is normalized to have unit

95% confidence interval. We obtained a good fit of these classification images with the signal (Fig. 6D) using a scaling factor of the signal as a free parameter. The adjusted R^2 values were: 0.6 (JC), 0.69 (VM), and 0.86 (average).

Figs. 6E–G represent the classification images for detecting contrast modulations. These classification images contain a few significant components which are approximately symmetrical in respect to the fixation point (distance 0). The thick line in Fig. 6H illustrates the template of the linear ideal-observer (the side-band component of the contrast modulations) and the thin

Table 2
Statistical analysis of the best fitting values of the free parameters and the adjacent variance R^2 of the PTM and elaborated LAM shown in Table 1

	First-order	Second-order	<i>p</i>
	Mean ± 95%CI	Mean ± 95%CI	
PTM			
R^2	0.992 ± 0.010	0.978 ± 0.011	0.0064
γ	1.256 ± 0.083	1.432 ± 0.155	0.0497
<i>m</i>	0.150 ± 0.013	0.231 ± 0.092	0.0519
<i>k</i>	0.269 ± 0.087	0.064 ± 0.030	0.0023 ^a
N_{add}	3.83 ± 0.33	20.00 ± 4.44	0.0012 ^a
ELAM			
R^2	0.987 ± 0.010	0.940 ± 0.060	0.0645
<i>U</i>	2 ± 0	2 ± 0	
<i>m</i>	0.130 ± 0.050	0.144 ± 0.049	0.5123
<i>k</i>	0.713 ± 0.157	0.215 ± 0.100	0.0011 ^a
N_{add}	3.14 ± 0.57	9.81 ± 2.55	0.0032 ^a

^a Probabilities which are significant at $p = 0.05$ applying a Bonferoni correction.

line shows the template of the non-linear ideal observer (the modulating signal). The fit of the data with the side-band component yielded relatively high adjusted R^2 values: 0.42 (JC), 0.61 (VM), and 0.63 (average). The fit with the modulating signal was not possible without zeroing the scaling factor. These results show that the observers used the side-band component of the contrast modulations of 2 c/deg for detecting the second-order pattern.

4. Discussion

Burgess and Ghandeharian (1984) have shown that when humans are given sufficient a priori information of signal parameters they can detect luminance signals by making use of a cross-correlation algorithm. The present results have revealed that human observers are

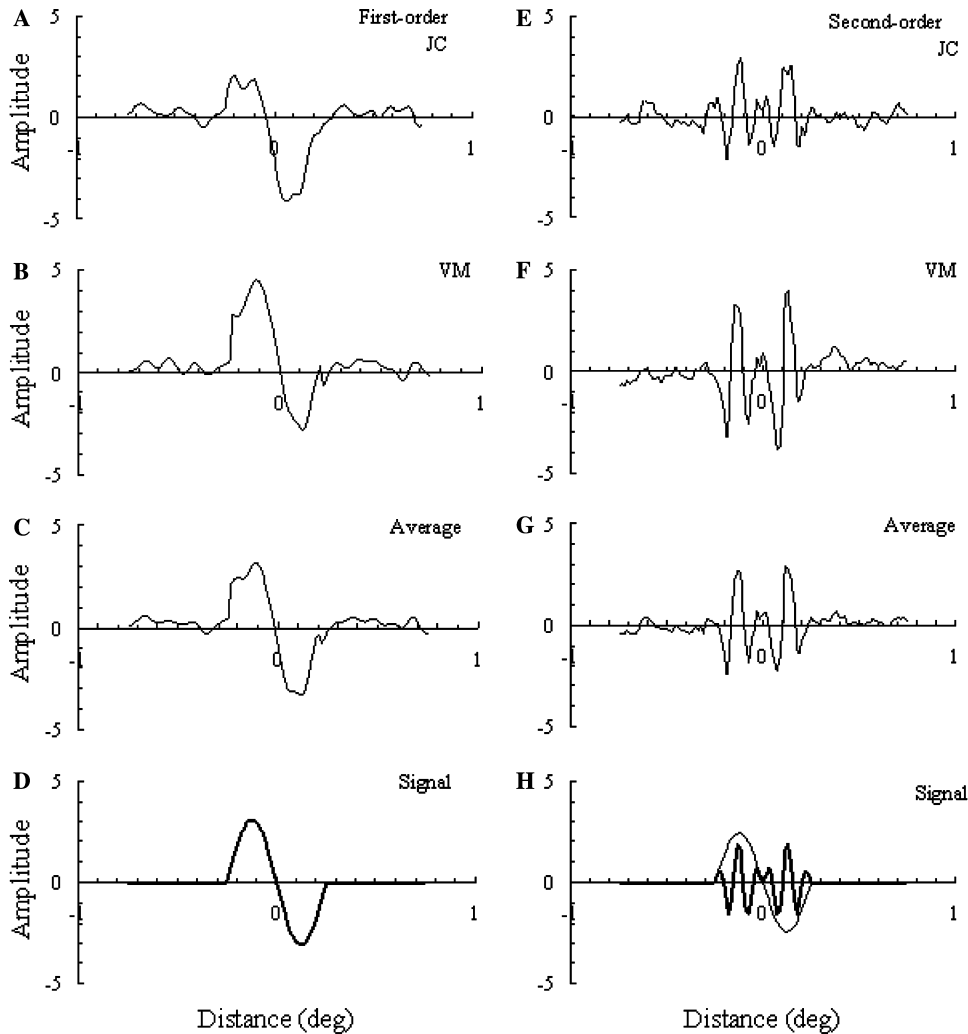


Fig. 6. Classification images for luminance (A–C) and contrast modulations (E–G) of 2 c/deg. The amplitude of the classification images is normalized to have unit 95% confidence interval. First row—data for observer JC, second row—data for observer VM, third row—averaged data, fourth row—luminance signal (D) and signals used by a linear ideal observer (thick line) and non-linear ideal observer (thin line).

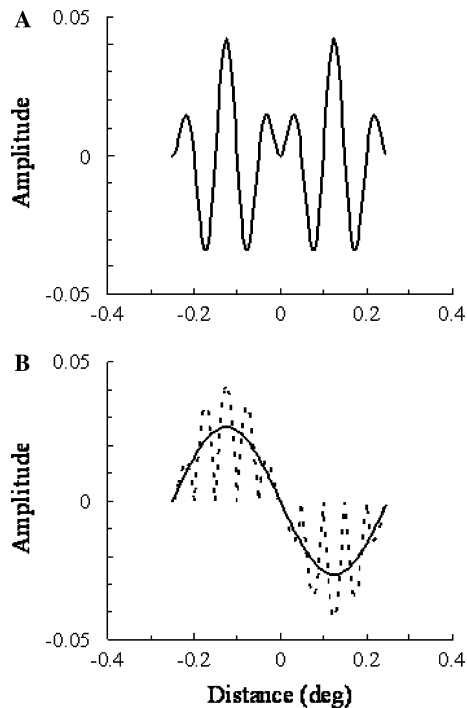


Fig. 7. One dimensional spatial profiles of the templates used by ideal observers for detecting contrast modulations. (A) Template of a linear ideal-observer model, (B) template of a non-linear ideal-observer model (thick line) and the output of the non-linear device of this model (dashed line).

also able to do phase-sensitive detection of both luminance and contrast modulations when there is a priori information of signal parameters.

To compare the efficiencies for detecting first- and second-order patterns, we considered two ideal-observer models for the detection of contrast modulations. One of them is the standard ideal observer who detects a luminance signal known exactly by cross-correlating the received stimulus with a copy of the signal (Green & Swets, 1974). In the case of a 2AFC experiment for detection of contrast modulations of a sinusoidal carrier, the template of this ideal observer is the side-band component of the contrast modulations (Appendix A, Fig. 7A). The second model is influenced by models for detecting second-order modulations which assume the existence of a distinct non-linear second-order pathway (Cavanagh & Mather, 1989; Chubb & Sperling, 1988; Wilson et al., 1992). The main feature of these models is that a non-linearity introduces a spectral component at the modulating frequency which is extracted by a linear filter tuned to that frequency. The template of such an ideal observer whose matching device is preceded by a full-wave non-linearity has the waveform of the modulating signal (Appendix A, Fig. 7B, solid line). Given the same contrast modulations, the linear ideal observer has 10% higher performance than the non-linear ideal observer.

We found a high overall efficiency for detection of luminance patterns ($\eta = 0.18\text{--}0.2$). These findings are consistent with estimates of efficiency for luminance gratings by others (Burgess, Wagner, Jennings, & Barlow, 1981; Kersten, 1983, 1984). Using the predictions of the more efficient linear ideal-observer model for contrast modulations, we found that the overall efficiency for luminance patterns was higher than that for contrast modulations ($\eta = 0.036\text{--}0.042$).

To establish the factors limiting performance in the detection of second-order information, we measured d' for detecting signals of 0.6 and 2 c/deg embedded in fixed and different static Gaussian noise. The data were analysed by two real-observer models: the perceptual template model (Lu & Dosher, 1999) and the elaborated linear amplifier model (Eckstein et al., 1997). With approximately similar accuracy, both models have shown that the detection of second-order patterns is characterised by lower sampling efficiency and higher additive internal noise than the detection of first-order stimuli. The other two parameters of the perceptual template model, the coefficient determining the equivalent multiplicative noise (m) and the exponent of the power transducer function (γ) for both first- and second-order signals were not significantly different. Similar results for the parameter m were obtained by the elaborated linear amplifier model. With this model, the effects of sampling efficiency and internal noise on detection performance can be separated from the effects due to stimulus uncertainties. The results have shown that uncertainty numbers (U) for both first- and second-order signals were not significantly different. This implies that the internal noise components induced by the external noise and the signal and the decision variables monitored by the observers are similar for both types of modulations.

The classification images have revealed that the side-band component of contrast modulations is likely to be used as a template in the detection process. Such a template could be physiologically implemented by a combination of two channels whose linear receptive fields have spatial frequencies of 8 ($f_c - f_m$) and 12 c/deg ($f_c + f_m$). This conclusion, however, is not likely to be applicable for the case of contrast modulations of binary noise. The side-band signal of this type of second-order modulations contains multiple side-band components and, therefore, the template would consist of multiple channels. In such a case, the observers might use a distinct non-linear second-order pathway whose template is a copy of the modulation signal. This suggestion, however, needs further research to be verified.

We found that the d' values for phase-certain and phase-uncertain conditions (signal/pedestal phase difference of 0 and 180 deg) were significantly different for luminance modulations of 0.6 and 2 c/deg and contrast modulations of 0.6 c/deg, while those for contrast modulations of 2 c/deg differed with a marginal probability

of 0.054. Kersten (1983) measured performance for detection of luminance gratings embedded in noise with and without a priori phase information. He found that prior knowledge of phase improved performance for detection of 0.5 and 2 c/deg, but this effect was significant only for the lower spatial frequency. In our experiment, the signals were added to a pedestal and this could explain the stronger effect of a prior knowledge of phase on the discriminating luminance patterns of 2 c/deg. The small effect of a priori phase information on the discriminating contrast-modulated increments of 2 c/deg might be due to lower phase sensitivity for this type of spatial pattern.

Burgess and Colborne (1988) measured human performance for the detection of sinusoidal gratings in a 2AFC experiment with two identical noise samples (twin noise) and found that performance improved by a factor of 1.6 over the condition with different noise samples. Watson, Taylor, and Borthwick (1997) found that performance in detecting Gabor patches embedded in fixed noise samples was better than in different- and twin-noise conditions, but some experience with the noise sample was required. Beard and Ahumada (1999) also reported that fixed noise conditions resulted in lower thresholds than twin noise. They suggested that the fixed/twin effect is due to template learning. In our experiments we used fixed noise conditions which showed better performance than different-noise conditions. We attribute this effect to the cross-correlation performance which depends on the multiplicative component of the internal noise due to the external noise, but not on the external noise itself. Our observers were able to familiarise themselves with the fixed-noise samples, however, longer practice may also increase the fixed-noise effect.

It should be noted that contrast sensitivities and spatial integration windows for first- and second-order modulations are different. Our conclusions are based on the results obtained by the stimuli used in the present experiments. Contrast modulations of a carrier having a different spatial frequency, or stimuli of different spatial sizes might be detected with different efficiencies.

In conclusion, the present results have shown that both first- and second-order pathways can detect signals by applying a similar phase-sensitive (cross-correlation) algorithm. This means that humans can have higher detection performance for objects defined by luminance and contrast modulations if they have sufficient a priori information of the object parameters. We found that the detection of second-order patterns had lower sampling efficiency and higher additive internal noise as compared to the detection of first-order stimuli. The classification images for contrast modulations revealed that real observers use a template which is similar to the side-band component of the contrast modulations. This finding suggests that human observers can detect contrast

modulations of a sinusoidal carrier using two first-order channels whose linear receptive fields are tuned to the spatial frequencies of the side-band component of the second-order pattern. The lower sensitivity of the mechanism detecting second-order patterns might be due to higher levels of additive internal noise and lower sampling efficiency than those of the mechanism analysing first-order patterns.

Acknowledgments

This research was supported by a BBSRC Grant (223/S13702). We thank the anonymous reviewers for their valuable comments and suggestions.

Appendix A

We present ideal-observer and energy models for discriminating incremental luminance modulations added to a luminance pedestal and incremental contrast modulations added to a contrast-modulated pedestal. These models were used to fit the data of Experiment 1.

A.1. Ideal-observer model for discriminating luminance modulations

Consider a 2AFC experiment in which both stimulation fields contain different Gaussian noise samples (n_1 and n_2) and a sinusoidal pedestal [$P \sin(2\pi f_m)$] of contrast P and spatial frequency f_m . One of the fields contains a luminance sinusoidal signal [$M \sin(2\pi f_m)$] the other one has no signal. The ideal observer is presented with a priori information of signal parameters and has to select the correct field. In such conditions, one possibility is that the ideal observer subtracts one field from the other and correlates the result with a template that matches the signal:

$$\text{Field 1: } M \sin(2\pi f_m) + P \sin(2\pi f_m) + n_1,$$

$$\text{Field 2: } P \sin(2\pi f_m) + n_2.$$

The output correlation is

$$\begin{aligned} R &= \{M \sin(2\pi f_m) + P \sin(2\pi f_m) + n_1 \\ &\quad - [P \sin(2\pi f_m) + n_2]\} \otimes M \sin(2\pi f_m) \\ &= \{[M \sin(2\pi f_m) + n_1 - n_2]\} \otimes M \sin(2\pi f_m) \\ &= M \sin(2\pi f_m) \otimes M \sin(2\pi f_m) + n_{12} \otimes M \sin(2\pi f_m), \end{aligned} \quad (\text{A.1})$$

where \otimes denotes correlation and $n_{12} = n_1 - n_2$. The polarity of the output correlation is used to select the correct alternative. If $R > 0$ then the signal is presented in the field 1; if $R < 0$ then the signal is presented in the field 2.

When the signal is specified exactly and the output correlation is Gaussian distributed, d' can be expressed as (Burgess, 1990; Pelli, 1990):

$$d' = \left(\frac{E}{N} \right)^{1/2}, \quad (\text{A.2})$$

where E is the energy of the incremental signal (the integral of the squared luminance function) and N is the density of the external noise.

A.2. Ideal-observer models for discriminating contrast modulations

Let us now apply this ideal-observer approach for discriminating a contrast-modulated increment $[C \sin(2\pi f_c)(1 + M \sin(2\pi f_m))]$ superimposed on a contrast-modulated pedestal from the contrast-modulated pedestal which are embedded in Gaussian white noise:

Field 1: $C \sin(2\pi f_c)[1 + P \sin(2\pi f_m) + M \sin(2\pi f_m)] + n_1$

Field 2: $C \sin(2\pi f_c)[1 + P \sin(2\pi f_m)] + n_2$.

The cross-correlation detector uses a template (T) which is the difference between the stimuli presented in fields 1 and 2

$$\begin{aligned} T &= C \sin(2\pi f_c)[1 + P \sin(2\pi f_m) + M \sin(2\pi f_m)] \\ &\quad - C \sin(2\pi f_c)[1 + P \sin(2\pi f_m)] \\ &= C \sin(2\pi f_c)M \sin(2\pi f_m). \end{aligned} \quad (\text{A.3})$$

The output correlation is

$$\begin{aligned} R &= \{C \sin(2\pi f_c)[1 + P \sin(2\pi f_m) + M \sin(2\pi f_m)] \\ &\quad + n_1 - C \sin(2\pi f_c)[1 + P \sin(2\pi f_m)] - n_2\} \\ &\quad \otimes C \sin(2\pi f_c)M \sin(2\pi f_m) \\ &= \{[C \sin(2\pi f_c)M \sin(2\pi f_m) + n_1 - n_2] \\ &\quad \otimes C \sin(2\pi f_c)M \sin(2\pi f_m) \\ &= C \sin(2\pi f_c)M \sin(2\pi f_m) \\ &\quad \otimes C \sin(2\pi f_c)M \sin(2\pi f_m) + n_{12} \\ &\quad \otimes C \sin(2\pi f_c)M \sin(2\pi f_m)\}. \end{aligned} \quad (\text{A.4})$$

The template of this ideal observer is the side-band component of the incremental contrast modulations which can be expressed as the difference between two cosine signals whose frequencies are $(f_c - f_m)$ and $(f_c + f_m)$ (Fig. 7A)

$$\begin{aligned} &C \sin(2\pi x f_c)M \sin(2\pi x f_m) \\ &= \frac{CM}{2} \{\cos[2\pi(f_c - f_m)] - \cos[2\pi(f_c + f_m)]\}. \end{aligned} \quad (\text{A.5})$$

Psychophysical and electrophysiological results have suggested that contrast modulations can be extracted by a distinct second-order pathway which consists of first-stage linear filters followed by a non-linearity and a second stage of linear filtering (Cavanagh & Mather,

1989; Chubb & Sperling, 1988; Wilson et al., 1992). In accordance with these suggestions, we could assume that contrast modulations are detected by a non-linear ideal observer who consists of a non-linear device followed by a matching device. The non-linear device is approximated by a full-wave (absolute value) rectifier whose output (A_{nl}) is the difference between the stimuli presented in the two fields (Fig. 7A, dashed line)

$$\begin{aligned} A_{nl} &= |C \sin(2\pi f_c)[1 + P \sin(2\pi f_m) + M \sin(2\pi f_m)]| \\ &\quad - |C \sin(2\pi f_c)[1 + P \sin(2\pi f_m)]| \\ &= |C \sin(2\pi f_c)| * |[1 + P \sin(2\pi f_m) + M \sin(2\pi f_m)]| \\ &\quad - |C \sin(2\pi f_c)| * |[1 + P \sin(2\pi f_m)]| \\ &= |C \sin(2\pi f_c)| * \{|[1 + P \sin(2\pi f_m) + M \sin(2\pi f_m)]| \\ &\quad - |[1 + P \sin(2\pi f_m)]|\} \\ &= |C \sin(2\pi f_c)|M \sin(2\pi f_m), \end{aligned} \quad (\text{A.6})$$

where we have used that

$$\begin{aligned} &|[1 + P \sin(2\pi f_m) + M \sin(2\pi f_m)]| - |[1 + P \sin(2\pi f_m)]| \\ &= 1 + P \sin(2\pi f_m) + M \sin(2\pi f_m) - 1 - P \sin(2\pi f_m) \\ &= M \sin(2\pi f_m), \end{aligned}$$

since $P + M = 1$ and $|\cdot|$ stands for the absolute-value operator.

The solid line in Fig. 7B illustrates the template of the matching device which is the A_{nl} component at the modulation spatial frequency (f_m). Its spatial profile was calculated by standard Fourier filtering of A_{nl} which removed the higher frequency components due to the carrier. An appropriate spatial smoothing of the signal A_{nl} can also remove the ripples due to the carrier. It should be noted that the template signal has lower amplitude than that of the carrier envelope. This difference is due to the presence of the valleys in the carrier profile.

The output correlation performed by the matching device whose template is denoted by T_{nl} can be expressed as follows:

$$\begin{aligned} R &= \{ |C \sin(2\pi f_c)[1 + P \sin(2\pi f_m) + M \sin(2\pi f_m)]| \\ &\quad + n_1 - |C \sin(2\pi f_c)[1 + P \sin(2\pi f_m)]| - n_2 \} \otimes T_{nl} \\ &= [C |\sin(2\pi f_c)|M \sin(2\pi f_m) + n_1 - n_2] \otimes T_{nl} \\ &= C |\sin(2\pi f_c)|M \sin(2\pi f_m) \otimes T_{nl} + n_{12} \otimes T_{nl}. \end{aligned} \quad (\text{A.7})$$

It should be noted that Eq. (A.7) is based on the assumption that Gaussian noise of zero mean is added after the non-linearity. This assumption is in line with the general model for observer performance (Kontsevich, Chen, & Tyler, 2002) in which the noise in the internal response at the decision stage could be approximated by only one noise source (critical noise) preceded by a non-linearity. If the Gaussian noise was added prior to the non-linearity, the rectified noise would have a non-Gaussian distribution of non-zero mean. Thus the requirement that the signal plus noise and the noise are Gaussian distributed would be violated.

We performed Matlab simulations of the output correlations produced by the linear [Eq. (A.4)] and non-linear [Eq. (A.7)] ideal-observer models for discriminating contrast modulations. Given the same stimulus parameters, the d' values calculated by the linear ideal-observer model were only 10% higher than the d' values estimated by the non-linear ideal-observer model. Similar d' values were obtained by using Eq. (A.2) and corresponding values of the signal contrast energy.

A.3. Energy model

When phase information is not available, the ideal observer uses a phase-insensitive energy strategy (Burgess & Ghandeharian, 1984; Green & Swets, 1974, pp. 211–217). The discrimination performance of the energy detector is based on the difference in energy (ΔE) between the two alternatives which can be expressed as (Burgess & Ghandeharian, 1984):

$$\begin{aligned} \Delta E &= [E_s + E_p + 2E_p^{1/2}E_s^{1/2} \cos(\theta)] - E_p \\ &= E_s + 2E_p^{1/2}E_s^{1/2} \cos(\theta), \end{aligned} \quad (\text{A.8})$$

where E_s and E_p are the energies of the signal and the pedestal and θ is the difference between the spatial phases of the signal and the pedestal. If the signal/pedestal contrast ratio is 7/9, the energy difference and d' are zero at $\theta = 112.5$ deg (Burgess & Ghandeharian, 1984).

Appendix B

We describe two real-observer models for detecting visual stimuli which are used to fit the data of Experiment 2.

Models based on statistical decision theory (Barlow, 1978; Legge et al., 1987; Pelli, 1991) have assumed that human performance for the detection of first-order patterns embedded in Gaussian noise is limited by two main factors: an additive internal noise (N_{add}) whose amplitude does not depend on the input and a suboptimal sampling efficiency (k) with which humans use the available stimulus information. Human performance of real observers was modelled by including these factors in the equation describing the performance of an ideal observer Eq. (A.2):

$$d'_d = \left(\frac{kE}{N + N_{\text{add}}} \right)^{1/2}. \quad (\text{B.1})$$

This linear amplifier model, however, cannot explain the estimated higher detection performance when the signal is embedded in fixed noise as compared to that in the presence of different noise. Burgess and Colborne (1988) have shown that d' for detection of sinusoidal gratings in a 2AFC experiment in the presence of fixed noise was higher by a factor of 1.6 than that measured

in conditions with different noise. They suggested the existence of a multiplicative component of internal noise which is proportional to external noise density.

Lu and Doshier (1999) proposed a perceptual template model for the detection of first-order patterns which is based on the LAM and observations in pattern vision and pattern masking. The PTM consists of: (i) a perceptual template, (ii) a non-linear transducer function, (iii) a multiplicative internal noise whose amplitude is a monotonic function of the energy of the signal and external noise, (iv) an additive internal noise source, and (v) a decision process. According to the PTM, Eq. (B.1) could be modified as follows:

$$d'_d = \frac{(kE)^{\gamma/2}}{[N^\gamma + mN^\gamma + m(kE)^\gamma + N_{\text{add}}]^{1/2}}, \quad (\text{B.2})$$

where γ is the exponent of the power transducer function, m is a coefficient which determines the equivalent multiplicative noises due to the external noise and the signal.

In a 2AFC experiment, if both images are embedded in fixed noise, the difference between the noise samples in each field is zero and the output correlation does not depend on the external noise. In such a case, d'_f depends on the multiplicative components of the internal noise induced by the external noise (mN^γ) and the signal energy [$m(kE)^\gamma$], but not on the external noise itself

$$d'_f = \frac{(kE)^{\gamma/2}}{[mN^\gamma + m(kE)^\gamma + N_{\text{add}}]^{1/2}}. \quad (\text{B.3})$$

Eckstein et al. (1997) proposed an elaborated LAM which consists of additive and multiplicative noise sources and a decision process with stimulus uncertainties. The amplitude of the multiplicative internal noise in this model is proportional only to the power of the external noise. To make a comparison between the PTM and the elaborated LAM, we assume that the amplitude of the multiplicative internal noise is a function of the amplitudes of the signal and the external noise. Therefore, the elaborated LAM can be used to calculate d' by Eqs. (B.2) and (B.3), setting $\gamma = 1$. This model approximates the nonlinearities of the transducer functions by the properties of an equivalent uncertainty process. To this end, the internal d' measure is converted to percent-correct performance in the presence of uncertainty, which can be expressed as follows:

$$\begin{aligned} Pc(M, U, d') &= \int_{-\infty}^{\infty} g(x - d') [G(x)]^{M(1+U)-1} \\ &\quad + Ug(x) [G(x)]^{M(1+U)-2} G(x - d') dx, \end{aligned} \quad (\text{B.4})$$

where $g(x) = \sqrt{\frac{1}{2\pi}} \exp[-\frac{x^2}{2}]$, $G(x) = \int_{-\infty}^x g(y) dy$, M is the number of possible signal locations ($M = 2$ in the case of a 2AFC task) and U is the uncertainty number corresponding to the irrelevant decision variables per location monitored by the observer.

References

- Abbey, C. K., & Eckstein, M. P. (2002). Classification image analysis: Estimation and statistical inference for two-alternative forced-choice experiments. *Journal of Vision*, 2, 66–78.
- Ahumada, A. J. Jr., (1996). Perceptual classification images from vernier acuity masked by noise. *Perception*, 26(Suppl.), 18.
- Ahumada, A. J. Jr., (2002). Classification image weights and internal noise level estimation. *Journal of Vision*, 2, 121–131.
- Ahumada, A. J., Jr., & Lovell, J. (1971). Stimulus features in signal detection. *Journal of the Acoustical Society of America*, 49, 1751–1756.
- Ahumada, A. J., Jr., Marken, T. R., & Sandusky, A. (1975). Time and frequency analyses of auditory signal detection. *Journal of the Acoustical Society of America*, 57, 385–390.
- Barlow, H. B. (1978). The efficiency of detecting changes of density in random dot patterns. *Vision Research*, 18, 637–650.
- Beard, B. L., & Ahumada, A. J. Jr., (1999). Detection in fixed and random noise in foveal and parafoveal vision explained by template learning. *Journal of the Optical Society of America A*, 16, 755–763.
- Burgess, A. E., & Colborne, B. (1988). Visual signal detection. IV. Observer inconsistency. *Journal of the Optical Society of America A*, 5, 617–627.
- Burgess, A. E. (1990). High level visual decision efficiencies. In C. Blakemore (Ed.), *Vision: Coding and efficiency* (pp. 431–440). New York: Cambridge University Press.
- Burgess, A. E., Wagner, R. F., Jennings, R. J., & Barlow, H. B. (1981). Efficiency of human visual signal discrimination. *Science*, 214, 93–94.
- Burgess, A., & Ghandeharian, H. (1984). Visual signal detection. I. Ability to use phase information. *Journal of the Optical Society of America A*, 1, 900–905.
- Cavanagh, P., & Mather, G. (1989). Motion: The long and short of it. *Spatial Vision*, 4, 103–129.
- Chubb, C., & Sperling, G. (1988). Drift-balanced random stimuli: a general basis for studying non-Fourier motion perception. *Journal of the Optical Society of America A*, 5, 1986–2007.
- Daugman, J. G., & Downing, C. J. (1995). Demodulation, predictive coding, and spatial vision. *Journal of the Optical Society of America A*, 12, 641–660.
- Eckstein, M. P., Ahumada, A. J., Jr., & Watson, A. B. (1997). Visual signal detection in structured backgrounds. II. Effects of contrast gain control, background variations, and white noise. *Journal of the Optical Society of America A*, 14, 2406–2419.
- Green, D. B., & Swets, J. A. (1974). *Signal detection theory and psychophysics*. New York: Wiley.
- Judd, C. M., & McClelland, G. H. (1989). *Data analysis: A model comparison approach*. New York: Harcourt Brace Jovanovich.
- Kersten, D. J. (1983). *A comparison of human and ideal performance for the detection of visual patterns*. PhD Dissertation, University of Minnesota, Minnesota.
- Kersten, D. J. (1984). Spatial summation in visual noise. *Vision research*, 24, 1977–1990.
- Kontsevich, L. L., Chen, C.-C., & Tyler, C. W. (2002). Separating the effects of response nonlinearity and internal noise psychophysically. *Vision Research*, 42, 1771–1784.
- Legge, G., Kersten, D., & Burgess, A. E. (1987). Contrast discrimination in noise. *Journal of the Optical Society of America A*, 4, 391–406.
- Levitt, H. (1971). Transformed up-down methods in psychoacoustics. *Journal of the Acoustic Society of America A*, 49, 467–477.
- Lu, Z. L., & Dosher, B. A. (1999). Characterizing human perceptual inefficiencies with equivalent internal noise. *Journal of the Optical Society of America A*, 16, 764–778.
- Macmillan, N. A., & Creelman, C. D. (1991). *Detection theory: A user's guide*. New York: Cambridge University Press.
- Manahilov, V., Calvert, J., & Simpson, W. A. (2003). Temporal properties of the visual responses to luminance and contrast modulated noise. *Vision Reserach*, 43, 1855–1867.
- Nagaraja, N. S. (1964). Effect of luminance noise on contrast thresholds. *Journal of the Optical Society of America A*, 54, 950–955.
- Pelli, D. G. (1990). The quantum efficiency of vision. In C. Blakemore (Ed.), *Vision: Coding and efficiency* (pp. 3–24). New York: Cambridge University Press.
- Pelli, D. G. (1991). Noise in the visual system may be early. In M. Landy & J. A. Movshon (Eds.), *Computational Models of Visual Processing* (pp. 147–152). Cambridge: MIT Press.
- Pelli, D. G., & Zhang, L. (1991). Accurate control of contrast on microcomputer displays. *Vision Research*, 31, 1337–1350.
- Schofield, A. J., & Georgeson, M. A. (1999). Sensitivity to modulations of luminance and contrast in visual white noise: separate mechanisms with similar behaviour. *Vision Research*, 39, 2697–2716.
- Schofield, A. J., & Georgeson, M. A. (2000). The temporal properties of first- and second-order vision. *Vision Research*, 40, 2475–2487.
- Simpson, W. A., Falkenberg, H. K., & Manahilov, V. (2003). Sampling efficiency and internal noise for motion detection, discrimination and summation. *Vision Research*, 43, 2125–2132.
- Tanner, W. P., Jr., & Birdsall, T. G. (1958). Definitions of d' and η as psychophysical measures. *Journal of the Acoustic Society of America A*, 30, 922–928.
- Watson, A. B., Taylor, M., & Borthwick, R. (1997). *Image quality and entropy masking proceedings, human vision, visual processing, and digital display VIII*, San Jose, CA, SPIE, Bellingham, WA, 3016, pp. 2–12.
- Wilson, H. R., Ferrera, V. P., & Yo, C. (1992). A psychophysically motivated model for two-dimensional motion perception. *Visual Neuroscience*, 9, 79–97.